Applied Surface Science 535 (2021) 147727

Contents lists available at ScienceDirect

Applied Surface Science

journal homepage: www.elsevier.com/locate/apsusc

# Reactivity of different nitriding agents with chlorine-terminated surface during atomic layer deposition of silicon nitride

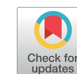

Tirta Rona Mayangsari[a], Luchana Lamierza Yusup[b], Romel Hidayat[b], Tanzia Chowdhury[b], Young-Kyun Kwon[c], Won-Jun Lee[b,*]

[a] Department of Chemistry, Universitas Pertamina, Jl. Teuku Nyak Arief, Simprug, Jakarta, Indonesia
[b] Department of Nanotechnology and Advanced Materials Engineering, Sejong University, Seoul 05006, Republic of Korea
[c] Department of Physics and Research Institute for Basic Sciences, Kyung Hee University, Seoul 02447, Republic of Korea

ARTICLE INFO

*Keywords:*
Atomic layer deposition
Silicon nitride
Density functional theory
Surface reaction
Chlorine-terminated surface
Nitriding agent

ABSTRACT

The atomic layer deposition (ALD) of silicon nitride using silicon chloride was simulated by density functional theory (DFT) calculation to compare different nitriding agents. We chose the $NSiCl_2$*/SiCl*-terminated $Si_3N_4$ substrate as the adequate chlorine-terminated substrate. We confirmed that the thermal ALD reaction using $NH_3$ or $N_2H_4$ is energetically favorable and found that the reaction with $N_2H_4$ shows an activation energy of 1.77 eV, which is lower than 3.30 eV of the reaction with $NH_3$. In the plasma-enhanced ALD (PEALD) process using $NH_3$ plasma, $NH_2^-$ ion and H· radical remove the Cl atoms of the $Si_3N_4$ surface to form active sites for the following reaction, –$SiNH_2$* group or –Si*. N· radicals in $N_2$ plasma may not remove the Cl atoms because the recombination reaction is more favored. The PEALD process using $NH_3$ plasma showed a growth rate of 0.09 nm/cycle at 300 °C, but the growth rate of the process using $N_2$ plasma is negligible, which is in good agreement with our DFT calculations.

## 1. Introduction

Silicon nitride has unique properties, such as high etching selectivity against silicon oxide or silicon [1], superior diffusion barrier against copper, alkali ions, dopants, or moisture, high dielectric constant, and high charge trap density [2,3]. The primary application of silicon nitride in the semiconductor manufacturing process includes the sidewall spacer of complementary metal-oxide-semiconductor (CMOS) devices [4], the dielectric barrier for copper interconnect [5], and the charge trap layer in three-dimensional NAND flash devices [6]. Silicon nitride thin films with excellent film quality have been produced by low-pressure chemical vapor deposition (LPCVD) techniques. However, the use of LPCVD is limited by the thermal budget and the step coverage in the fabrication of state-of-art semiconductor devices. Plasma-enhanced chemical vapor deposition (PECVD) can reduce the thermal budget. However, it produces silicon-rich silicon nitride film with lower film density and inadequate step coverage. In particular, the silicon nitride film prepared by PECVD contains a high concentration of hydrogen [3,7].

Recently, the atomic layer deposition (ALD) technique was adapted for better step coverage as well as better film quality at lower temperatures [8]. ALD is a thin-film deposition process in which two self-limiting half-reactions are repeated. The first half-reaction is the surface reaction of precursor molecules, while the second half-reaction is the surface reaction of co-reactant species. Therefore, the ALD reaction rate is dependent on the types of precursors, co-reactant, and surface active sites [9,10], so the co-reactant is as crucial as the precursor. Plasma-enhanced ALD (PEALD) differs from thermal ALD in that it uses the plasma activation of co-reactant in the second half-reaction. Although the thermal ALD process dominated the early years of research on the ALD of silicon nitride, the number of publications on the PEALD has increased rapidly in the last five years [11]. Silicon chloride precursors have been used for both thermal ALD and PEALD processes, while chlorine-free precursors have been reported for PEALD only [11,12]. Silicon nitride film has been deposited by thermal ALD using dichlorosilane ($SiH_2Cl_2$) or hexachlorodisilane ($Si_2Cl_6$) with ammonia ($NH_3$) gas at process temperatures of 450 °C or higher [8,11,13,14], and the PEALD using $Si_2Cl_6$ or $SiH_2Cl_2$ with $NH_3$ plasma showed lower deposition temperatures down to below 400 °C [15–17]. No thermal ALD process was reported using non-chloride precursors. However, the high reactivity of plasma species allows the use of non-chloride precursors in the deposition process. PEALD of silicon nitride were reported using trisilylamine (TSA) [18], neopentasilane [19], bis(*tert*-butylamino)silane (BTBAS) [20,21], tris(dimethylamino)silane

* Corresponding author.
*E-mail address:* wjlee@sejong.ac.kr (W.-J. Lee).

https://doi.org/10.1016/j.apsusc.2020.147727
Received 7 February 2020; Received in revised form 12 August 2020; Accepted 28 August 2020
Available online 03 September 2020
0169-4332/ © 2020 Elsevier B.V. All rights reserved.

(TDMAS) [22], Di(*sec*-butylamino)silane (DSBAS, $SiH_3N(^sBu)_2$) [23], bis(dimethylaminomethylsilyl)trimethylsilyl amine (DTDN2-H2) [6], and 1,3-di-isopropylamino-2,4-dimethylcyclosilazane (CSN-2) [24,25]. Experimental and theoretical studies comparing nitriding agents were reported for aminosilane precursors. Nitrogen ($N_2$) plasma gives the highest growth rate in PEALD using BTBAS, and $N_2/H_2$ or $NH_3$ plasma produces hydrogen-terminated silicon nitride surface, which hinders the chemisorption of aminosilane precursors [26]. Also, the $N_2$ plasma after the $NH_3$ plasma removes the surface hydrogen atoms to activate the chemisorption of aminosilane precursors [17,24,26]. However, the research for co-reactants for silicon chloride precursors is less active. $NH_3$ is the most commonly used co-reactant in thermal ALD and PEALD processes. The use of hydrazine ($N_2H_4$) in combination with $Si_2Cl_6$ was first reported at 600 °C, where pure ALD reaction was impossible [27]. A recent report indicates that the silicon nitride film can be prepared using $N_2H_4$ even at 275 °C [28], which is a much lower process temperature than with $NH_3$. There has been no report on ALD of silicon nitride using silicon chloride precursors with either $N_2$ gas or $N_2$ plasma.

In our previous works, we studied the first half-reaction of ALD silicon nitride using silicon chloride precursors by density functional theory (DFT) calculation to investigate the effects of surface-active sites and silicon chloride precursors on the ALD reaction [29,30]. In the present work, we studied the second-half reaction of ALD silicon nitride using silicon chloride also by DFT calculation to investigate different nitriding agents for silicon chloride precursors. The nitriding agent, the co-reactant for the ALD of silicon nitride, must replace chlorine atoms on the growing film surface with nitrogen-containing ligands. To mimic both the thermal ALD process and the PEALD process, we considered two types of nitriding agents, gas molecules and plasma species, respectively. $NH_3$, $N_2H_4$, and $N_2$ were considered as molecules, and $NH_2^-$, NH·, H·, $N^-$, and N· were considered as plasma species. We constructed and compared different chlorine-terminated surfaces to mimic the surface condition after the first half-reaction, and then studied the surface reactions on the stable but reactive chlorine-terminated surfaces. We simulated the surface reaction and the recombination reaction of nitriding agents and compared them in terms of reaction energy and activation energy.

## 2. Experimental

### 2.1. Calculations details.

DFT calculations were performed using Material Studio 7.0 with the $Dmol^3$ package (Accelrys BIOVIA, USA) [31,32]. Generalized gradient approximation (GGA) with Perdew-Burke-Ernzerhof (PBE) functional and double numerical polarization 4.4 basis set were used in all calculations [30–32]. DFT-D with Grimme method was used for the dispersion correction of the system.[33] The Brillouin zone integration was sampled within Monkhorst-Pack k-point meshes of 2 × 2 × 1 for all calculations. Octupole multipolar expansion was applied for more precise results. Smearing of $9 \times 10^{-4}$ Ha (Hartree, 27.21 eV) and dipole slab correction in the orbital occupancy scheme were applied. We used a customized quality of convergence tolerance without symmetry constraint until the total energy change was converged to $10^{-6}$ Ha, and all the atomic forces became smaller than $2 \times 10^{-4}$ Ha·Å$^{-1}$.

Chlorine-terminated surfaces were constructed by adding chlorine atoms or silicon chloride groups to the top layer of the $Si_3N_4$ substrate. The substrate consisted of 4 layers of (2 × 2) supercell of β-$Si_3N_4$ (0 0 1) plane and was described in detail elsewhere [29]. We constructed $N_2$, $NH_3$, and $N_2H_4$ molecules as the gas species of the nitriding agents and constructed various ionic or neutral fragments of $NH_3$ or $N_2$ to represent the plasma species [34–38]. The $NH_3$ molecule, $NH_2^-$ ion, NH·, and H· radicals were considered as major $NH_3$ plasma species, while $N_2$ molecule, $N^-$ ion, and N· radical were considered as $N_2$ plasma species. For $NH_3$ plasma, we considered $NH_2^-$ ion because it is generated at a high density in RF plasma, as shown in Eq. (1) [36,39]:

$$NH_3 + e^- \rightarrow NH_2^- + H\cdot \quad (1)$$

At the same time, hydrogen radical is also produced by the reaction of Eq. (1). The NH· radical is formed by the dissociation of an $NH_3$ molecule into an NH· radical and two H· radicals, as indicated in Eq. (2) [35,38]:

$$NH_3 + e^- \rightarrow NH\cdot + 2H\cdot + e^- \quad (2)$$

The density of NH· radical is lower than those of $NH_2^-$ ion and H· radical. For $N_2$ plasma, we considered both $N^-$ ion and N· radical because they have high densities in RF plasma, as shown in Eq. (3) [38]:

$$N_2 + e^- \rightarrow N^- + N\cdot \quad (3)$$

We simulated the reaction of a single ion or radical with the chlorine-terminated silicon nitride surface. We computed the adsorption energy ($E_{ads}$), the reaction energy ($E_R$), and activation energy ($E_A$) using Eqs. (4), (5), and (6):

$$E_{ads} = E_{physisorption} - E_{unbound\ reactant} \quad (4)$$

$$E_R = E_{chemisorption} - E_{physisorption} \quad (5)$$

$$E_A = E_{transition\ state} - E_{physisorption} \quad (6)$$

where $E_{unbound\ reactant}$, $E_{physisorption}$, $E_{transistion\ state}$, and $E_{chemisorption}$ are the total energies of the system calculated during the surface reactions for the states before and after the physisorption, at transition, and after the chemisorption, respectively. For a surface reaction where the physisorption state is absent, the energy of reaction was determined by the difference between the state before physisorption and the state after chemisorption. The details of our calculations can be found in our previous study on the reaction between silicon chloride precursors and silicon nitride surfaces [29,30]. We also simulated the surface reaction as well as the recombination of two ions or radicals to expect if the recombination reaction of the plasma species is favorable.

### 2.2. ALD process of silicon nitride

We used a traveling-wave-type cold wall reactor equipped with a plasma source (13.56 MHz of capacitively-coupled plasma) to deposit silicon nitride film. $Si_2Cl_6$ (UP Chemical Co., Korea) was used as the silicon precursor while $NH_3$ (99.9995%) and $N_2$ (99.9995%) were used as the nitriding agents. The silicon nitride films were deposited at 300 °C with plasma RF power of 100 W under 1.5 Torr for 50 cycles. The details of the experimental conditions are described elsewhere [29].

## 3. Results and discussion

### 3.1. Construction of chlorine-terminated silicon nitride surfaces

Since there has been no report on the modeling of chlorine-terminated silicon nitride surfaces, we prepared chlorine-terminated surface structures by attaching chlorine atoms or silicon chloride groups on silicon nitride surfaces in several ways and tried to obtain stable structures by geometry optimization. In the previous work [29], we modeled hydrogen-terminated $Si_3N_4$ surfaces to study the surface reaction of silicon precursors. First, we constructed the bare $Si_3N_4$ surface by stacking four slabs of (2 × 2) supercell without any modification, resulting in under-coordinated ⟩Si=N– bonds on the surface. Next, the NH*/SiH*-terminated surface was constructed by passivating the bare $Si_3N_4$ surface using hydrogen atoms. The asterisk (*) indicates surface active sites. Finally, the NH*/SiNH$_2$*-terminated surface was transformed from the NH*/SiH*-terminated surface by replacing the H atom of Si–H* surface group by $NH_2$, assuming the exposure to $NH_3$ before the precursor supply. As an analogy of previous work, we first

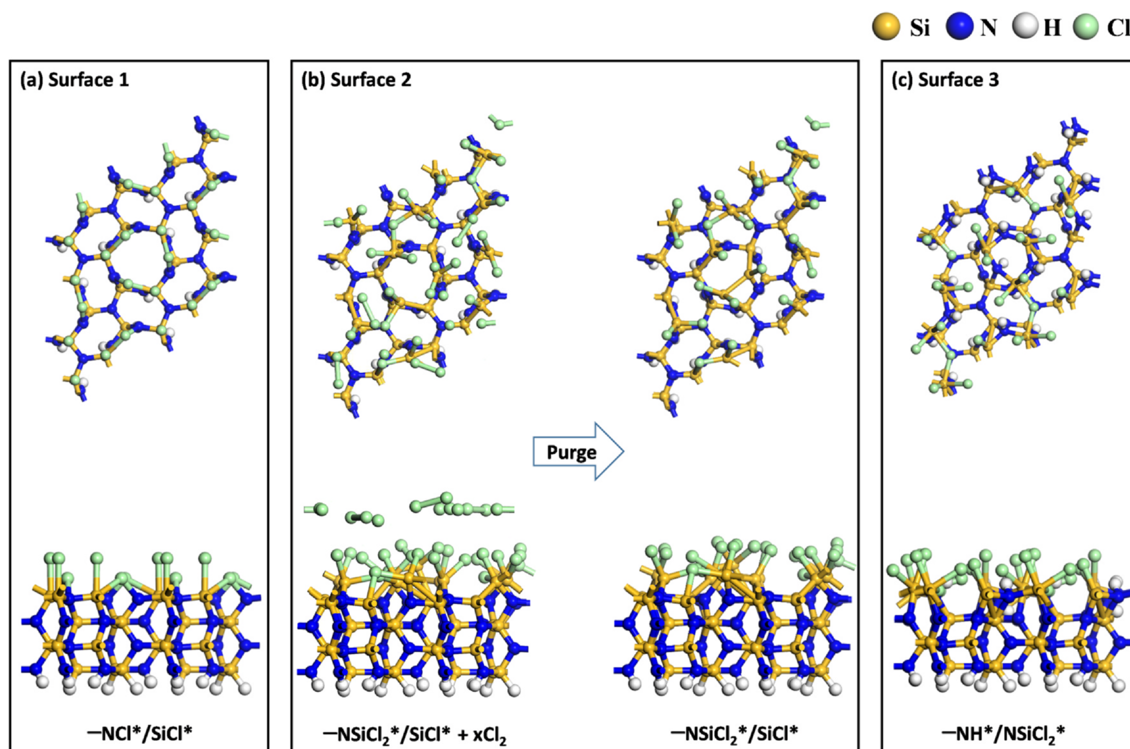


**Fig. 1.** Modeling of chlorine-terminated silicon nitride surface: (a) NCl*/SiCl*-terminated surface, (b) $NSiCl_2$*/SiCl*-terminated surface, and (c) NH*/$NSiCl_2$*-terminated surface. The asterisk (*) indicates surface active sites.

constructed different types of chlorine-terminated silicon nitride surfaces to model the surface reaction of nitriding agents, as shown in Fig. 1. The NCl*/SiCl*-terminated surface in Fig. 1(a), denoted as surface 1, was constructed by the passivating of the bare $Si_3N_4$ surface with chlorine atoms. However, it is unrealistic that the silicon chloride precursor will react with the silicon nitride surface to form NCl*. In the first half-reaction, the silicon chloride precursor, $SiCl_4$ or $Si_2Cl_6$, are chemisorbed on the nitrogen atoms of silicon nitride surface to form the NSiCl* surface groups [30,40] so that silicon chlorides would passivate all surface nitrogen atoms. The $NSiCl_2$*/SiCl*-terminated surface, denoted as surface 2, was transformed from the NCl*/SiCl*-terminated surface by replacing the Cl atom of N–Cl* with $SiCl_3$, as shown in Fig. 1(b). The optimized geometry shows that some Cl atoms interact with each other to form $Cl_2$ molecules, which are desorbed from the surface. By removing the $Cl_2$ molecules from the surface, a stable chlorine-terminated $Si_3N_4$ surface was obtained with $SiCl_2$* and SiCl* groups as the surface-active sites, as shown in Fig. 1(b). The combination of $SiCl_2$* and SiCl* groups on the silicon nitride surface is more stable than the $SiCl_3$* group due to the enlarged distance between the chlorine atoms. It can also be seen that the Si–Si bonds between $NSiCl_2$* and SiCl* were also formed to compensate for the displacement of Cl atoms from the silicon chloride groups. The NH*/$NSiCl_2$*-terminated surface denoted as surface 3 in Fig. 1(c) was constructed from the NH*/$SiNH_2$*-terminated surface in the previous work by replacing the H atoms of NH* and $SiNH_2$* with $SiCl_2$ groups. However, all surface hydrogen atoms could not be replaced by $SiCl_2$ because H atoms from the NH* groups were located slightly below $SiNH_2$*, which disagrees with the literature where the contamination of hydrogen was less than 10% [11,41]. Thus, the NH*/$NSiCl_2$* surface is not a good model for the calculation of ALD silicon nitride.

Surfaces 1 and 2 were examined for the second half-reaction study by calculating the surface reaction of an $NH_3$ molecule on both surfaces. Fig. 2 shows the total energies of the unbound, physisorption, transition state, and chemisorption structures for the reaction of an $NH_3$ molecule on surfaces 1 and 2. The calculation results on surface 1 show the exothermic physisorption of $NH_3$ with the total energy difference of −0.21 eV. Two different reaction pathways were assumed after physisorption. The assumption for the first pathway was the chemisorption of $NH_3$ to produce the Si–$NH_2$* surface group and an HCl molecule, as shown in Fig. 2(a). The chemisorption was exothermic with reaction energy of −4.04 eV and was accompanied by the formation of a $Cl_2$ molecule, as follows in Eq. (7):

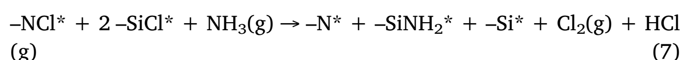

$$\text{–NCl* + 2 –SiCl* + NH}_3\text{(g)} \rightarrow \text{–N* + –SiNH}_2\text{* + –Si* + Cl}_2\text{(g) + HCl(g)} \quad (7)$$

Two Cl atoms from –NCl* and –SiCl* were combined to form a $Cl_2$ molecule, –N*, and –Si*, which shows that the NCl*/SiCl*-terminated surface is not stable during the ALD reaction. The transition state showed lower energy than the chemisorption state, so we assumed the transition state obtained from Eq. (7) as the reaction product of the second reaction pathway. $NH_2Cl$ and HCl molecules are formed by removal of Cl atoms from the surface, as shown in Eq. (8):

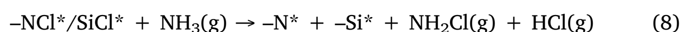

$$\text{–NCl*/SiCl* + NH}_3\text{(g)} \rightarrow \text{–N* + –Si* + NH}_2\text{Cl(g) + HCl(g)} \quad (8)$$

The calculation showed a stronger exothermic reaction with a total energy difference of −4.57 eV and activation energy of −0.15 eV, indicating that the reaction should be fast (Fig. 2(b)). However, the result disagrees with the experimental observations where the ALD of silicon nitride using $NH_3$ gas requires a rather high temperature of 450 °C or higher [11]. Therefore, the NCl*/SiCl*-terminated surface is not a correct model to simulate the second half-reaction of ALD silicon nitride.

The reaction between $NH_3$ with surface 2, the $NSiCl_2$*/SiCl*-terminated surface, was investigated analogously with the surface 1. The physisorption of the $NH_3$ molecule is exothermic, with the energy of −0.41 eV. Two different pathways were also assumed. For the first pathway, the $NH_3$ molecule chemisorbs by forming an –$NH_2$* surface group and an HCl molecule, as shown in Eq. (9). For the second pathway, the $NH_3$ removes two chlorine atoms from the surface to form $NH_2Cl$ and HCl molecules, as shown in Eq. (10):

**Fig. 2.** Energy diagram for the surface reactions of an $NH_3$ molecule on silicon nitride surfaces: (a) the formation of $–SiNH_2*$ on the NCl*/SiCl*-terminated surface, (b) the formation of an $NH_2Cl$ molecule on the NCl*/SiCl*-terminated surface, and (c) the formation of $–SiNH_2*$ on $NSiCl_2*$/SiCl*-terminated surface.

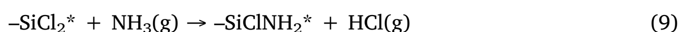

$$–SiCl_2* + NH_3(g) \rightarrow –SiClNH_2* + HCl(g) \quad (9)$$

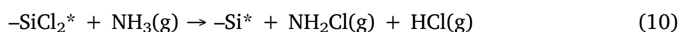

$$–SiCl_2* + NH_3(g) \rightarrow –Si* + NH_2Cl(g) + HCl(g) \quad (10)$$

The first pathway in Fig. 2(c) is an exothermic reaction with the reaction energy of −1.46 eV and an energy barrier of 3.30 eV. The chemisorption state in Fig. 2(c) shows that the chemisorption of $NH_3$ produces $–NH_2*$, the active surface site for the first half-reaction. Meanwhile, the second pathway was an endothermic reaction with the reaction energy of 2.02 eV (Fig. S1), which means the reaction is not favorable. Therefore, we chose surface 2, the $NSiCl_2*$/SiCl*-terminated surface, to compare nitriding agents in the following calculations.

According to our Mulliken charge analysis on the Cl-terminated surface, the Si atoms have positive charges (0.915 e or 0.829 e), while the Cl atoms have negative charges (−0.327 e). The N atom of $NH_3$ shows negative charges (−0.527 e), whereas the H atoms show positive charges (0.176 e). The N atom is attracted to the most positive Si atom on the surface, donating the electron and forming a bond. In the process of the reaction, charge transfers from the electronegative N atom of $NH_3$ to the Si atom of the surface, making Si more positive, N more negative in the product state.

### 3.2. *The surface reactions of $NH_3$ and $N_2H_4$ molecule*

We compared $N_2H_4$ gas with $NH_3$ gas as the nitriding agent for thermal ALD. We assumed two reaction pathways, as shown in Eqs. (11) and (12).

$$–SiCl* + N_2H_4(g) \rightarrow –SiNH_2* + NH_2Cl(g) \quad (11)$$

$$-2–SiCl* + N_2H_4(g) \rightarrow –Si* + NHCl(g) + NH_3(g) \quad (12)$$

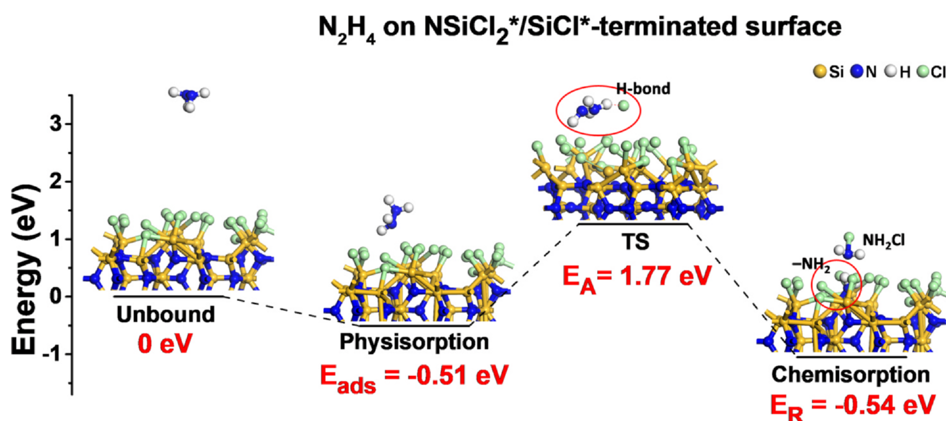


**Fig. 3.** Energy diagram for the surface reactions of an $N_2H_4$ molecule on the $NSiCl_2$*/SiCl*-terminated silicon nitride surface.

Fig. 3 shows the energy diagram for the surface reactions of an $N_2H_4$ molecule. The physisorption of $N_2H_4$ is more exothermic than that of $NH_3$ with the energy of −0.51 eV. The chemisorption of $N_2H_4$ in Eq. (11) was exothermic, with the reaction energy of −0.54 eV and the energy barrier of 1.77 eV. The reaction of $N_2H_4$ is less exothermic than that of $NH_3$ due to the less stable byproduct, $NH_2Cl$. The energy barrier for $N_2H_4$ is only half as compared with $NH_3$, indicating that the $N_2H_4$ reaction is faster than the $NH_3$ reaction. The optimized geometry of the transition state in Fig. 3 shows the elongated N–N bond of $N_2H_4$ and the formation of a hydrogen bond between the $NH_2$ and Cl atom from the surface. The transition state geometry for the $NH_3$ reaction showed the breaking of the N–H bond, as shown in Fig. 2(c). The hydrogen bond in Fig. 3 stabilized the molecular geometry at the transition state, corresponding to the lower energy barrier of $N_2H_4$ than that of $NH_3$. We also simulated the other pathway where an $N_2H_4$ molecule abstract chlorine atom from the surface to form NHCl and $NH_3$ molecules, as shown in Eq. (12). The reaction is endothermic with the reaction energy of 2.12 eV, indicating that the reaction was not favored (Fig. S2). Therefore, the first reaction pathway is plausible, and we confirmed that $N_2H_4$ is more reactive than $NH_3$ due to its lower energy barrier. We also can expect that $N_2H_4$ is more reactive than $NH_3$ based on the bond dissociation energy (BDE) values. The BDE values of the N–N and N–H bonds in $N_2H_4$ are around 2.82 eV and 3.51 eV [42], whereas the BDE of the N–H bond in $NH_3$ is about 4.6 eV [43].

### 3.3. $NH_3$ plasma surface reactions

The surface reactions of $NH_3$ plasma species were simulated, and the energy diagrams and the optimized geometries of the reactions are shown in Fig. 4. Both physisorption and chemisorption of $NH_2^-$ ion was exothermic with the energies of −0.33 eV and −0.90 eV, respectively, and the energy barrier for chemisorption was 0.29 eV. The optimized geometry of the transition state in Fig. 4(a) shows that the energy barrier corresponds to the migration of $NH_2^-$ ion closer to the silicon–silicon bridge surface group to form a Si–$NH_2$ surface group. The radical species, NH· and H·, also showed exothermic physisorption and chemisorption, as shown in Fig. 4(b) and (c). The energy barriers for chemisorption were small negative values, corresponding to high reaction rates. The NH· radical reacts with the surface to form the surface group of Si–NHCl*, and the Cl atom released from $SiCl_2$* migrates to neighboring –SiCl* to form $SiCl_2$*. The H· radical reacts with the surface to form an HCl molecule and reactive surface sites. As shown in Fig. 4(b) and (c), the optimized geometries of the transition states are similar to those of the physisorption ones without any significant changes.

When two radicals were introduced simultaneously into the simulation, either the chemisorption or the recombination of two radicals is possible. The energies for the chemisorption and the recombination of two NH· radicals were −8.55 eV and −5.81 eV (Fig. S3), indicating that the chemisorption is favored to form a Si–NH bridge and Si–NHCl surface groups. On the other hand, the energies for the chemisorption and the recombination of two H· radicals were −4.77 eV and −4.56 eV (Fig. S4), indicating that the recombination is less favored than the chemisorption. We did not consider the recombination of two ions, because Material Studio software does not allow two ions to have the same polarities. Also, the lifetime of $NH_2^-$ ion in plasma is longer than those of NH· and H· radicals [36], so the recombination of $NH_2^-$ ion would be less favored than the chemisorption. In summary, the $NH_2^-$ ion would chemisorb on the surface, and the H· radicals would remove the Cl atoms from the surface to form active surface sites.

### 3.4. $N_2$ Plasma surface reactions

The energy diagrams and the optimized geometries for the surface reactions of $N_2$ plasma species are shown in Fig. 5. We could not acquire the chemisorption of an $N_2$ molecule because of the inert nature of the $N_2$ molecule, as shown in Fig. 5(a). The N· radical shows exothermic physisorption and surface reaction with the energies of −2.86 eV and −0.77 eV, and the energy barrier was 0.40 eV, as shown in Fig. 5(b). The $N^-$ ion also shows an exothermic surface reaction with a very low activation energy of 0.02 eV, and we could not acquire the physisorption state after the geometry optimization, as shown in Fig. 5(c). Both N· radical and $N^-$ ion reacted with the Cl atom of the surface to form the NCl molecule as the reaction byproduct.

However, when two N· radicals were introduced simultaneously, the DFT calculation showed that the recombination reaction would be more favored than the surface reaction. Fig. 6 shows that the physisorption energy of two N· radicals was −0.14 eV, which is less exothermic than the physisorption of a single N· radical. The surface reaction of two N· in Fig. 6(a) yields the reaction energy of −0.47 eV, which is also less exothermic than the surface reaction of the single radical. Meanwhile, the recombination is very exothermic, with the reaction energy of −10.3 eV, as shown in Fig. 6(b), and energetically more favorable than the surface reaction. The energy for recombination agrees well with the dissociation energy of the N–N bond in $N_2$, which is 9.76 eV. N· radical or $N^-$ ion reacts with another radical or ion instead of electropositive Si atoms to lower the total system energy. Therefore, charge analysis is useful in explaining the reaction mechanism when combined with energy analysis, but not in all cases. It is reported that the lifetime of N· radical is very short in plasma [38], suggesting a good agreement with the favored recombination reactions of this work. These results indicate that $N_2$ plasma is less efficient than $NH_3$ plasma due to the recombination reactions when using silicon chloride precursors.

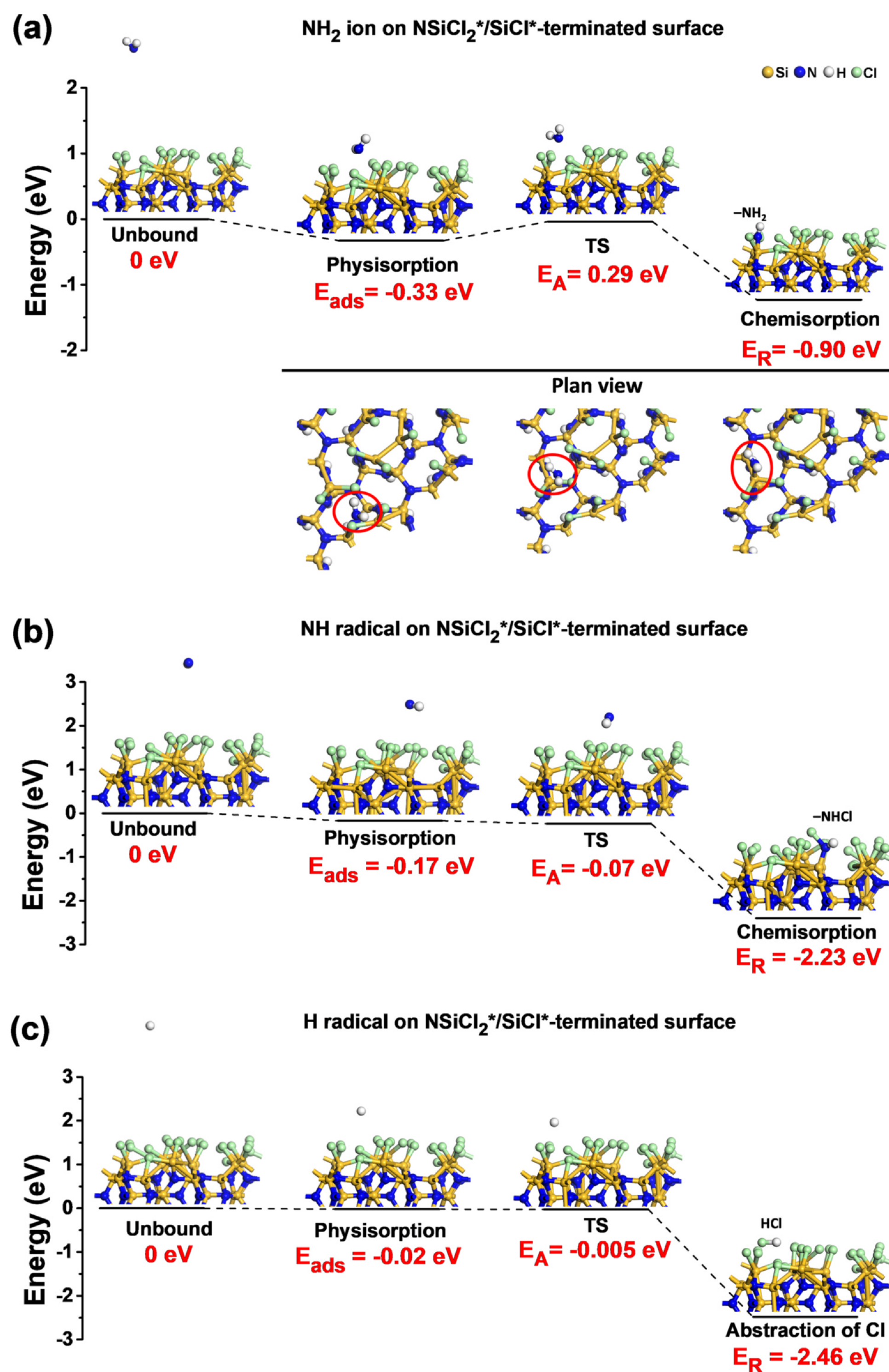


**Fig. 4.** Energy diagram for the surface reactions of $NH_3$ plasma species on the $NSiCl_2$*/SiCl*-terminated silicon nitride surface: (a) $NH_2^-$ ion, (b) NH· radical, and (c) H· radical.

*3.5. PEALD of silicon nitride using $NH_3$ and $N_2$ plasma.*

Fig. 7 shows the growth rate of ALD silicon nitride using $NH_3$ plasma and $N_2$ plasma. The growth rate was calculated by dividing the film thickness by the number of ALD cycles. The film thickness was around 4.5 nm when using the $NH_3$ plasma as the nitriding agent, giving a growth rate per cycle (GPC) of ~ 0.09 nm/cycle. However, the film thickness was 0.25 nm when using $N_2$ plasma, giving a negligible GPC of ~ 0.005 nm/cycle. These results show that $N_2$ plasma could not react efficiently with the chlorine-terminated surface, as suggested by the calculation. On the other hand, $NH_3$ gas or its plasma species will react with the chlorine-terminated surface to produce silicon nitride film.

## 4. Conclusion

We studied the second-half reaction of ALD silicon nitride using silicon chloride by DFT calculation to investigate different nitriding

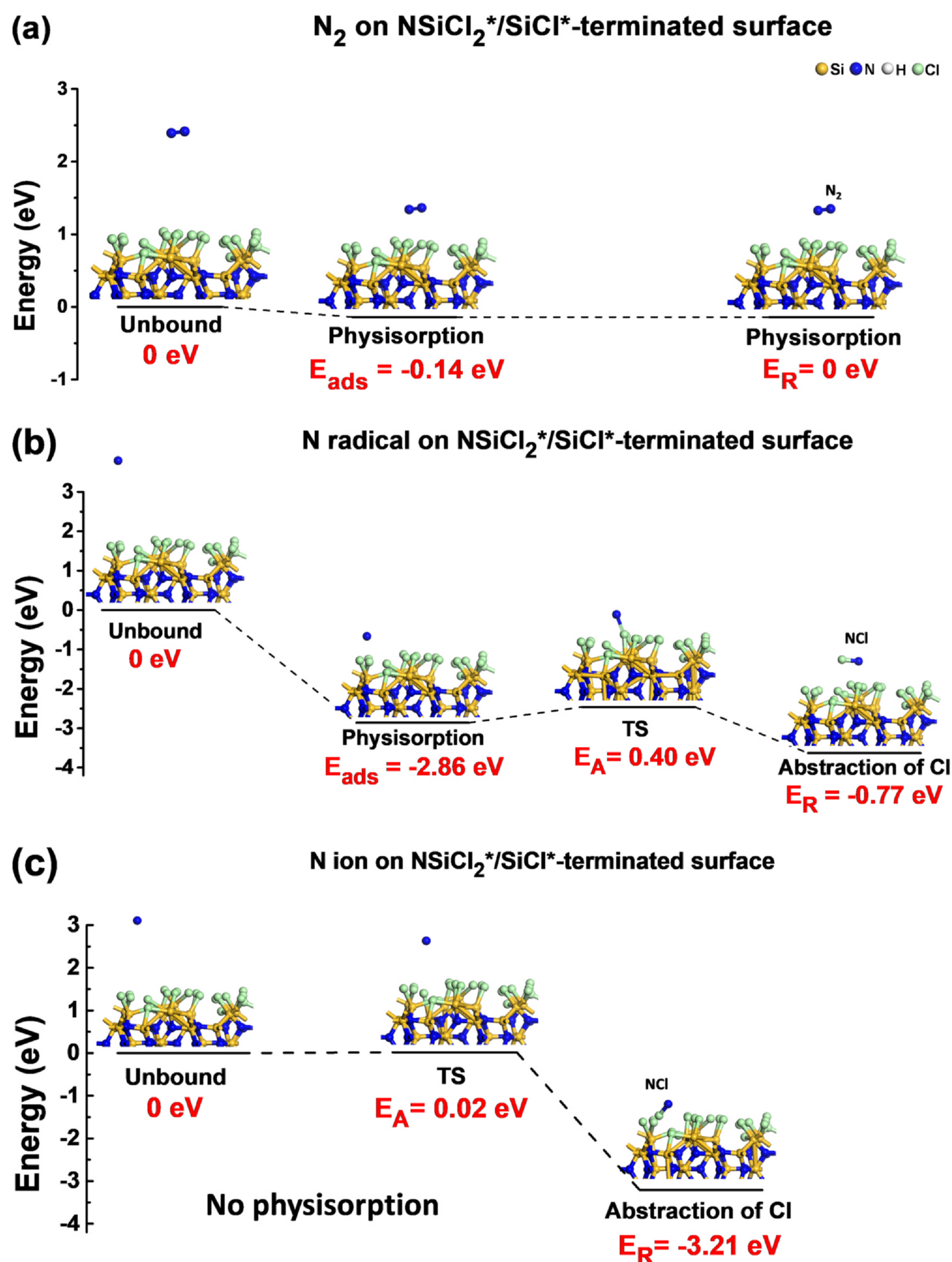


**Fig. 5.** Energy diagram for the surface reactions of $N_2$ plasma species on the $NSiCl_2$*/SiCl*-terminated silicon nitride surface: (a) $N_2$ molecule, (b) N· radical, and (c) $N^-$ ion.

agents. The construction of the chlorine-terminated surface is essential in predicting the reactivity of the nitriding agents, and the $NSiCl_2$*/SiCl*-terminated surface is the adequate surface, which is in a good agreement with the experimental observations found in the literature. Thermal ALD processes using $NH_3$ and $N_2H_4$ were energetically favorable, and the $N_2H_4$ molecule showed the energy barrier of 1.77 eV that is lower than 3.30 eV of $NH_3$. In plasma-enhanced ALD process using $NH_3$ plasma, $NH_2^-$ ion chemisorbs on the surface to form –$SiNH_2$* surface group, and H· radical removes the Cl atoms of the surface to form surface active sites for the following reaction. N· radicals in $N_2$ plasma are inadequate as nitriding agents in the ALD process using silicon chlorides because they favor the recombination reaction over the surface reaction. The PEALD process using $NH_3$ plasma showed a growth rate of 0.09 nm/cycle at 300 °C, but the growth rate of the process using $N_2$ plasma is negligible, which is in good agreement with our DFT calculations.

## CRediT authorship contribution statement

**Tirta Rona Mayangsari:** Conceptualization, Methodology, Software, Validation, Formal analysis, Investigation, Data curation, Writing - original draft, Visualization. **Luchana Lamierza Yusup:** Conceptualization, Methodology, Software, Formal analysis, Investigation, Data curation, Writing - original draft. **Romel Hidayat:** Validation, Writing - review & editing, Visualization. **Tanzia Chowdhury:** Validation, Writing - review & editing, Visualization. **Young-Kyun Kwon:** Conceptualization, Methodology, Formal analysis, Investigation, Writing - review & editing, Supervision. **Won-Jun Lee:** Conceptualization, Investigation, Resources, Data curation, Writing - original draft, Visualization, Supervision, Project administration, Funding acquisition.

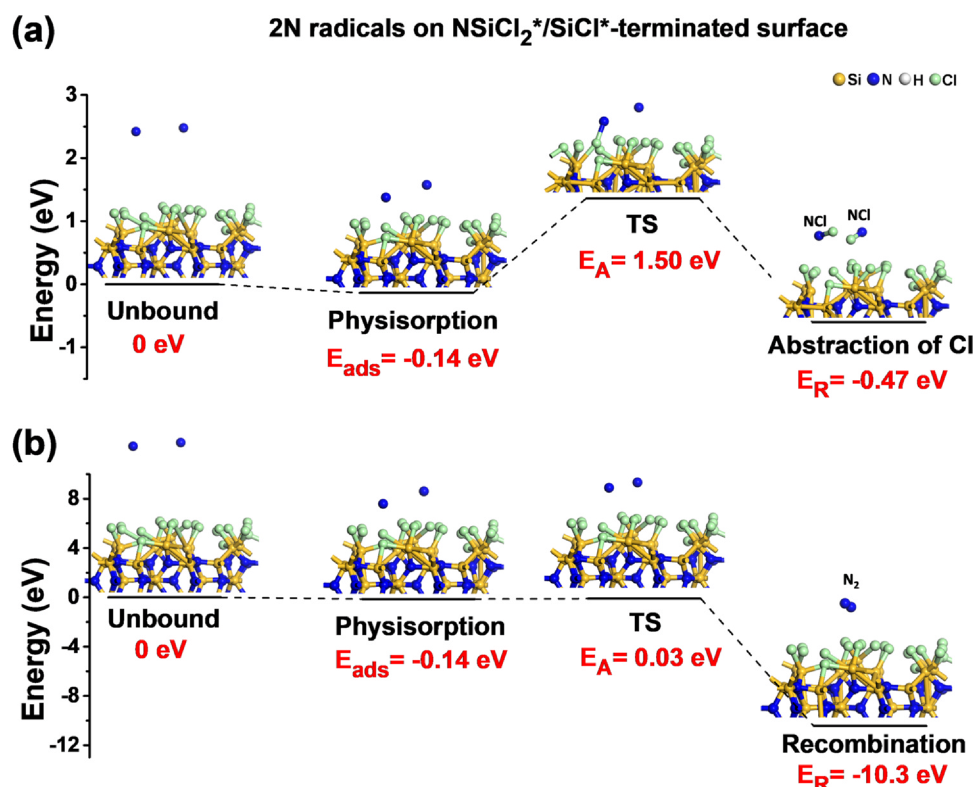


**Fig. 6.** Energy diagram for (a) the surface reaction and (b) the recombination of two N· radicals on the $NSiCl_2$*/SiCl*-terminated silicon nitride surface.

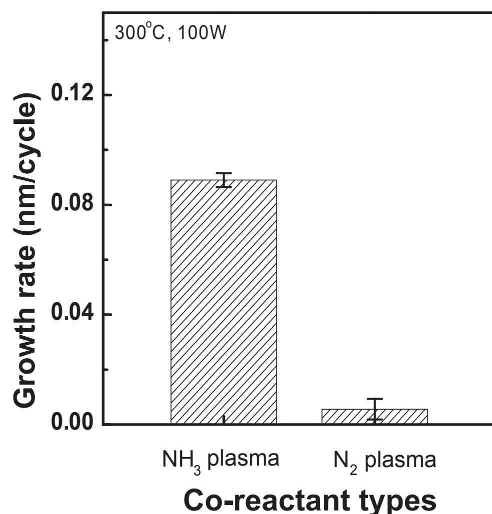


**Fig. 7.** The growth rates of PEALD silicon nitride at 300 °C using $NH_3$ plasma and $N_2$ plasma. $Si_2Cl_6$ was used as the silicon precursor.

## Declaration of Competing Interest

The authors declare that they have no known competing financial interests or personal relationships that could have appeared to influence the work reported in this paper.

## Acknowledgments

This work was supported by the faculty research fund of Sejong University, Republic of Korea in 2019.

## Appendix A. Supplementary material

Supplementary data to this article can be found online at https://doi.org/10.1016/j.apsusc.2020.147727.

## References

[1] S.D. Tzeng, S. Gwo, Charge trapping properties at silicon nitride/silicon oxide interface studied by variable-temperature electrostatic force microscopy, J. Appl. Phys. 100 (2006) 023711, , https://doi.org/10.1063/1.2218025.
[2] S. Kim, D.W. Kwon, S.H. Lee, S.K. Park, Y. Kim, H. Kim, Y.G. Kim, S. Cho, B.G. Park, Characterization of the vertical position of the trapped charge in charge-trap flash memory, J. Semicond. Technol. Sci. 17 (2017) 167–173, https://doi.org/10.5573/JSTS.2017.17.2.167.
[3] J.S. Kilby, Handbook of Semiconductor Manufacturing Technology, second ed., CRC Press of Taylor & Francis Group, Boca Raton, 2007. doi:10.1201/9781420017663.fmatt.
[4] K.J. Yang, T.J. King, C. Hu, S. Levy, H.N. Al-Shareef, Electron mobility in MOSFETs with ultrathin RTCVD silicon nitride/oxynitride stacked gate dielectrics, Solid. State. Electron. 47 (2003) 149–153, https://doi.org/10.1016/S0038-1101(02)00309-X.
[5] T.K.S. Wong, Time dependent dielectric breakdown in copper low-k interconnects: Mechanisms and reliability models, Materials (Basel). 5 (2012) 1602–1625, https://doi.org/10.3390/ma5091602.
[6] J.-M. Park, S.J. Jang, L.L. Yusup, W.-J. Lee, S.-I. Lee, Plasma-enhanced atomic layer deposition of silicon nitride using a novel silylamine precursor, ACS Appl. Mater. Interfaces. 8 (2016) 20865–20871, https://doi.org/10.1021/acsami.6b06175.
[7] C. Yang, J. Pham, Characteristic study of silicon nitride films deposited by LPCVD and PECVD, Silicon. 10 (2018) 2561–2567, https://doi.org/10.1007/s12633-018-9791-6.
[8] S.M. George, Atomic layer deposition: An overview, Chem. Rev. 110 (2010) 111–131, https://doi.org/10.1021/cr900056b.
[9] N.P. Dasgupta, H.-B.-R. Lee, S.F. Bent, P.S. Weiss, Recent advances in atomic layer deposition, Chem. Mater. 28 (2016) 1943–1947, https://doi.org/10.1021/acs.chemmater.6b00673.
[10] R.A. Ovanesyan, E.A. Filatova, S.D. Elliott, D.M. Hausmann, D.C. Smith, S. Agarwal, Atomic layer deposition of silicon-based dielectrics for semiconductor manufacturing: Current status and future outlook, J. Vac. Sci. Technol. A. 37 (2019) 060904, , https://doi.org/10.1116/1.5113631.
[11] X. Meng, Y.-C. Byun, H. Kim, J. Lee, A. Lucero, L. Cheng, J. Kim, Atomic layer deposition of silicon nitride thin films: a review of recent progress, challenges, and outlooks, Materials (Basel). 9 (2016) 1007, https://doi.org/10.3390/ma9121007.
[12] Y.J. Ji, K.S. Kim, K.H. Kim, J.Y. Byun, G.Y. Yeom, A brief review of plasma

enhanced atomic layer deposition of Si3N4, Appl. Sci. Converg. Technol. 28 (2019) 142–147, https://doi.org/10.5757/asct.2019.28.5.142.
[13] F.I. Riley, Silicon nitride and related materials, J. Am. Ceram. Soc. 83 (2000) 245–265, https://doi.org/10.1111/j.1151-2916.2000.tb01182.x.
[14] H. Klemm, Silicon nitride for high-temperature applications, J. Am. Ceram. Soc. 93 (2010) 1501–1522, https://doi.org/10.1111/j.1551-2916.2010.03839.x.
[15] W.J. Lee, U.J. Kim, C.H. Han, M.H. Chun, S.K. Rha, Y.S. Lee, Characteristics of silicon nitride thin films prepared by using alternating exposures of SiH2Cl2 and NH3, J. Korean Phys. Soc. 47 (2005) S598–S602 http://cat.inist.fr/?aModele=afficheN&cpsidt=17312105.
[16] R.A. Ovanesyan, D.M. Hausmann, S. Agarwal, Low-temperature conformal atomic layer deposition of SiNx films using $Si_2Cl_6$ and $NH_3$ plasma, ACS Appl. Mater. Interfaces. 7 (2015) 10806–10813, https://doi.org/10.1021/acsami.5b01531.
[17] X. Meng, H.S. Kim, A.T. Lucero, S.M. Hwang, J.S. Lee, Y.C. Byun, J. Kim, B.K. Hwang, X. Zhou, J. Young, M. Telgenhoff, Hollow cathode plasma-enhanced atomic layer deposition of silicon nitride using pentachlorodisilane, ACS Appl. Mater. Interfaces. 10 (2018) 14116–14123, https://doi.org/10.1021/acsami.8b00723.
[18] W. Jang, H. Jeon, C. Kang, H. Song, J. Park, H. Kim, H. Seo, M. Leskela, H. Jeon, Temperature dependence of silicon nitride deposited by remote plasma atomic layer deposition, Phys. Status Solidi. 211 (2014) 2166–2171, https://doi.org/10.1002/pssa.201431162.
[19] S. Weeks, G. Nowling, N. Fuchigami, M. Bowes, K. Littau, Plasma enhanced atomic layer deposition of silicon nitride using neopentasilane, J. Vac. Sci. Technol. A Vacuum, Surfaces, Film. 34 (2016) 01A140, https://doi.org/10.1116/1.4937993.
[20] H.C.M. Knoops, E.M.J. Braeken, K. de Peuter, S.E. Potts, S. Haukka, V. Pore, W.M.M. Kessels, Atomic layer deposition of silicon nitride from bis(tert -butylamino)silane and N2 plasma, ACS Appl. Mater. Interfaces. 7 (2015) 19857–19862, https://doi.org/10.1021/acsami.5b06833.
[21] R.H.E.C. Bosch, L.E. Cornelissen, H.C.M. Knoops, W.M.M. Kessels, Atomic layer deposition of silicon nitride from bis(tertiary-butyl-amino)silane and N2 plasma studied by in situ gas phase and surface infrared spectroscopy, Chem. Mater. 28 (2016) 5864–5871, https://doi.org/10.1021/acs.chemmater.6b02319.
[22] Y. Kim, J. Provine, S.P. Walch, J. Park, W. Phuthong, A.L. Dadlani, H.J. Kim, P. Schindler, K. Kim, F.B. Prinz, Plasma-enhanced atomic layer deposition of SiN-AlN composites for ultra low wet etch rates in hydrofluoric acid, ACS Appl. Mater. Interfaces. 8 (2016) 17599–17605, https://doi.org/10.1021/acsami.6b03194.
[23] T. Faraz, M. van Drunen, H.C.M. Knoops, A. Mallikarjunan, I. Buchanan, D.M. Hausmann, J. Henri, W.M.M. Kessels, Atomic layer deposition of wet-etch resistant silicon nitride using Di(sec -butylamino)silane and $N_2$ plasma on planar and 3D substrate topographies, ACS Appl. Mater. Interfaces. 9 (2017) 1858–1869, https://doi.org/10.1021/acsami.6b12267.
[24] J.M. Park, S.J. Jang, S.I. Lee, W.J. Lee, Novel cyclosilazane-type silicon precursor and two-step plasma for plasma-enhanced atomic layer deposition of silicon nitride, ACS Appl. Mater. Interfaces. 10 (2018) 9155–9163, https://doi.org/10.1021/acsami.7b19741.
[25] H. Cho, N. Lee, H. Choi, H. Park, C. Jung, S. Song, H. Yuk, Y. Kim, J.W. Kim, K. Kim, Y. Choi, S. Park, Y. Kwon, H. Jeon, Remote plasma atomic layer deposition of SiNx using cyclosilazane and H2/N2 plasma, Appl. Sci. 9 (2019) 3531, https://doi.org/10.3390/app9173531.
[26] C.K. Ande, H.C.M. Knoops, K. de Peuter, M. van Drunen, S.D. Elliott, W.M.M. Kessels, Role of surface termination in atomic layer deposition of silicon nitride, J. Phys. Chem. C. 6 (2015) 3610–3614, https://doi.org/10.1021/acs.jpclett.5b01596.
[27] S. Morishita, S. Sugahara, M. Matsumura, Atomic-layer chemical-vapor-deposition of silicon-nitride, Appl. Surf. Sci. 112 (1997) 198–204.
[28] D. Alvarez, J. Spiegelman, E. Heinlein, R. Holmes, C. Ramos, M. Leo, S. Webb, Novel oxidants and sources of nitrogen for atomic layer deposition, ECS Trans. 72 (2016) 243–248, https://doi.org/10.1149/07204.0243ecst.
[29] L.L. Yusup, J.-M. Park, Y.-H. Noh, S.-J. Kim, W.-J. Lee, S. Park, Y.-K. Kwon, Reactivity of different surface sites with silicon chlorides during atomic layer deposition of silicon nitride, RSC Adv. 6 (2016) 68515–68524, https://doi.org/10.1039/C6RA10909H.
[30] L.L. Yusup, J.-M. Park, T.R. Mayangsari, Y.-K. Kwon, W.-J. Lee, Surface reaction of silicon chlorides during atomic layer deposition of silicon nitride, Appl. Surf. Sci. 432 (2017) 127–131, https://doi.org/10.1016/j.apsusc.2017.06.060.
[31] B. Delley, An all-electron numerical method for solving the local density functional for polyatomic molecules, J. Chem. Phys. 92 (1990) 508–517, https://doi.org/10.1063/1.458452.
[32] B. Delley, From molecules to solids with the DMol3 approach, J. Chem. Phys. 113 (2000) 7756–7764, https://doi.org/10.1063/1.1316015.
[33] E.R. McNellis, J. Meyer, K. Reuter, Azobenzene at coinage metal surfaces: Role of dispersive van der Waals interactions, Phys. Rev. B - Condens. Matter Mater. Phys. 80 (2009) 1–10, https://doi.org/10.1103/PhysRevB.80.205414.
[34] P.R. McCurdy, C.I. Butoi, K.L. Williams, E.R. Fisher, Surface interactions of $NH_2$ radicals in $NH_3$ plasmas, J. Phys. Chem. B. 103 (1999) 6919–6929, https://doi.org/10.1021/JP9909558.
[35] P.J. Van Den Oever, J.H. Van Helden, C.C.H. Lamers, R. Engeln, D.C. Schram, M.C.M. Van De Sanden, W.M.M. Kessels, Density and production of NH and $NH_2$ in an Ar-$NH_3$ expanding plasma jet, J. Appl. Phys. 98 (2005) 093301, , https://doi.org/10.1063/1.2123371.
[36] A. Fateev, F. Leipold, Y. Kusano, B. Stenum, E. Tsakadze, H. Bindslev, Plasma chemistry in an atmospheric pressure Ar/$NH_3$ dielectric barrier discharge, Plasma Process. Polym. 2 (2005) 193–200, https://doi.org/10.1002/ppap.200400051.
[37] D.J.V. Pulsipher, E.R. Fisher, $NH_2$ and NH surface production in pulsed $NH_3$ plasmas on $TiO_2$: a steady-state probe of short pulse plasmas, Plasma Process. Polym. 10 (2013) 6–18, https://doi.org/10.1002/ppap.201200060.
[38] M. Sode, W. Jacob, T. Schwarz-Selinger, H. Kersten, Measurement and modeling of neutral, radical, and ion densities in H2–N2-Ar plasmas, J. Appl. Phys. 117 (2015) 083303, , https://doi.org/10.1063/1.4913623.
[39] W. Zheng, D. Jewitt, Y. Osamura, R.I. Kaiser, Formation of nitrogen and hydrogen-bearing molecules in solid ammonia and implications for solar system and interstellar ices, Astrophys. J. 674 (2008) 1242–1250, https://doi.org/10.1086/523783.
[40] R.A. Ovanesyan, D.M. Hausmann, S. Agarwal, A three-step atomic layer deposition process for SiNx using $Si_2Cl_6$, $CH_3NH_2$, and $N_2$ plasma, ACS Appl. Mater. Interfaces. 10 (2018) 19153–19161, https://doi.org/10.1021/acsami.8b01392.
[41] H.C.M. Knoops, K. de Peuter, W.M.M. Kessels, Redeposition in plasma-assisted atomic layer deposition: Silicon nitride film quality ruled by the gas residence time, Appl. Phys. Lett. 107 (2015) 014102, , https://doi.org/10.1063/1.4926366.
[42] M.W. Schmidt, M.S. Gordon, The decomposition of hydrazine in the gas phase and over an iridium catalyst, Zeitschrift Fur Phys. Chemie. 227 (2013) 1301–1336, https://doi.org/10.1524/zpch.2013.0404.
[43] J.G. Speight, Properties of atoms, radicals, and bonds, LANGE'S Handb. Chem, 17th ed.,, McGraw-Hill Education, 2016, p. 1104, , https://doi.org/10.1002/anie.200352070.